

Ultrafast Dynamics of Carrier Multiplication in Quantum Dots

Franz Schulze,^{1,*} Mario Schoth,¹ Ulrike Woggon,² Carsten Weber,¹ and Andreas Knorr¹

¹*Institut für Theoretische Physik, Nichtlineare Optik und Quantenelektronik, Technische Universität Berlin, Hardenbergstr. 36, 10623 Berlin, Germany*

²*Institut für Optik und Atomare Physik, Nichtlineare Optik, Technische Universität Berlin, Straße des 17. Juni 135, 10623 Berlin, Germany*

(Dated: May 27, 2011)

A quantum-kinetic approach to the ultrafast dynamics of carrier multiplication in semiconductor quantum dots is presented. We investigate the underlying dynamics in the electronic subband occupations and the time-resolved optical emission spectrum, focusing on the interplay between the light-matter and the Coulomb interaction. We find a transition between qualitatively differing behaviors of carrier multiplication, which is controlled by the ratio of the interaction induced time scale and the pulse duration of the exciting light pulse. On short time scales, i.e., before intraband relaxation, this opens the possibility of detecting carrier multiplication without referring to measurements of (multi-)exciton lifetimes.

PACS numbers: 78.47.jd, 78.67.Hc, 73.22.Dj

I. INTRODUCTION

Typically, in a semiconductor excited by a single photon, the conversion efficiency of light energy into electrical energy is strongly limited by the fact that per photon only a single electron-hole pair (or exciton) can be created. For single-junction solar cells, this determines the well-known Shockley-Queisser limit.¹ Using multiple materials with different band gaps (multi-junction cells), a larger part of the solar spectrum can be covered, and thus the conversion efficiency can be increased beyond this limit. Another way is to use materials which exhibit the creation of multiple excitons per incident photon (multiple-exciton generation - MEG), thus increasing the quantum yield for incident photons with energies higher than twice the band gap. For this reason, carrier multiplication is currently the subject of intensive investigation in nanostructures such as graphene structures^{2,3} and semiconductor quantum dots (QDs).⁴⁻¹⁴

Most of the experimental investigations focus on the decay dynamics of the carrier population in the conduction band as a measure of MEG: While an exciton decays radiatively on a time scale of tens to hundreds of picoseconds, multiexcitations can decay much faster (on a picosecond time scale) due to additional Coulomb-mediated impact ionization and Auger scattering channels. Thus, the detection of different decay time constants in dependence on the incident light frequency is used as an indication and quantitative measure of MEG. One disadvantage of these approaches is the ambiguity accompanying the discrimination of MEG from other effects in quantum dots such as charged excitons.⁴⁻⁶

Corresponding to experimental investigations, theory has focused on calculations of (multi-)exciton decay rates which were found to be crucial for MEG and its efficiency in concrete material systems.^{7,8} The theoretical descriptions are typically restricted to Bloch equations including phenomenological scattering rates as well as pseudo-potential approaches without quantum-kinetic time res-

olution of the carrier multiplication process. The time dynamics of absorption bleaching was investigated by Shabaev et al. in Ref. 9.

Here, we present a quantum-kinetic approach to carrier multiplication in a semiconductor QD including the time dynamics of the relevant Coulomb processes (impact ionization and Auger recombination), studied in the electronic occupations and the time-resolved optical emission spectrum. We propose that distinct quantum-kinetic signatures of the carrier dynamics due to different dynamical paths can be used as an experimental verification of carrier multiplication via the time-resolved optical emission in quantum dot structures: This proposal is, in principle, advantageous compared to measurements of exciton or multiexciton decay times due to a clear interpretation of the signal.

II. MODEL SYSTEM

The QD model underlying this work consists of eight electronic states exhibiting spin degeneracy, i.e., four in the conduction (c) and four in the valence band (v), depicted schematically in Fig. 1(a). The conduction band states are labeled by $|c\lambda s\rangle$, while the valence band states are labeled by $|v\lambda s\rangle$; here, λ denotes the subband index (two subband states for each band) and s the spin index.

The full system Hamiltonian reads

$$H = H_0 + H_{\text{cl}} + H_{\text{Coul}}, \quad (1)$$

where H_0 represents the free kinetics of the electrons:

$$H_0 = \sum_{\substack{\lambda=1,2 \\ s=\uparrow,\downarrow}} \left(\epsilon_{\lambda s}^c a_{c\lambda s}^\dagger a_{c\lambda s} + \epsilon_{\lambda s}^v a_{v\lambda s}^\dagger a_{v\lambda s} \right). \quad (2)$$

$a_{c\lambda s}^\dagger$ ($a_{v\lambda s}^\dagger$) and $a_{c\lambda s}$ ($a_{v\lambda s}$) are the creation and annihilation operators of an electron in the conduction (valence)

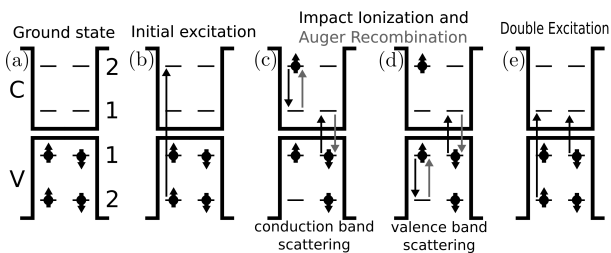


FIG. 1: (a) Quantum dot model in its ground state consisting of eight electronic states [four in the conduction (c) and four in the valence band (v)] exhibiting spin degeneracy. (b) Creation of an electron density in the state $|c2\uparrow\rangle$ by a classical light pulse. (c) Impact ionization (black) and Auger recombination (grey) due to energy-conserving conduction band electron-electron scattering. (d) Impact ionization (black) and Auger recombination (grey) due to energy-conserving electron-electron scattering in the valence band. (e) Simultaneous excitation of two electrons from the valence to the conduction band.

band and subband λ with spin s and energy $\epsilon_{\lambda s}^{c(v)}$, respectively.

Initially, the systems is excited by a classical light pulse close to the transition $|v2\uparrow\rangle \rightarrow |c2\uparrow\rangle$ [Fig. 1(b)], creating the single-exciton state $|c2\uparrow v2\uparrow\rangle$: This interaction between the electrons and the incident light pulse is treated semiclassically and in dipole and rotating wave approximation:

$$H_{cl} = M_{2\uparrow 2\uparrow}^{cv} E(t) a_{c2\uparrow}^\dagger a_{v2\uparrow} + \text{h.a.}, \quad (3)$$

where $E(t)$ is the classical light field at the QD location, taken to be a Gaussian pulse $E(t) = \tilde{E}(t) \cos(\omega_L t)$ with $\tilde{E}(t) = E_0 \exp\{-t^2/\tau^2\}$, with the pulse width τ . The pulse area is defined via the envelope of the pulse, $\theta = \int_{-\infty}^{\infty} dt' M_{2\uparrow 2\uparrow}^{cv} \tilde{E}(t')/\hbar$. $M_{2\uparrow 2\uparrow}^{cv}$ is the dipole matrix element of the considered transition.

To focus on the underlying dynamics of MEG, the full carrier-carrier interaction Hamiltonian is restricted for large parts of the article to the impact ionization (II) and Auger recombination (AR) processes of conduction band electrons, depicted in Fig. 1(c). The additional consideration of II and AR of valence band electrons [Fig. 1(d)], which occurs on an equal footing, complicates the presentation of the underlying physics while it does not qualitatively change the observed phenomena. For completeness, we include calculations of both scattering processes at the end of the numerical discussion including a comparison between the system dynamics excluding and including II and AR processes of valence band electrons.

The impact ionization process annihilates electrons in the states $|c2\uparrow\rangle$ and $|v1\downarrow\rangle$ and creates electrons in the multi-carrier state $|c1\uparrow c1\downarrow\rangle$ [black arrows in Fig. 1(c)], thus describing the transition between the single-exciton state $|c2\uparrow v2\uparrow\rangle$ and the two-exciton state $|c1\uparrow c1\downarrow v1\downarrow v2\uparrow\rangle$. The Auger recombination as the inverse process is described by the Hermitian adjoint [grey arrows in Fig. 1(c)]. The corresponding carrier-carrier interaction

Hamiltonian reads

$$H_{\text{Coul}} = V^{\text{II}} a_{c1\uparrow}^\dagger a_{c1\downarrow}^\dagger a_{v1\downarrow} a_{c2\uparrow} + V^{\text{AR}} a_{c2\uparrow}^\dagger a_{v1\downarrow}^\dagger a_{c1\downarrow} a_{c1\uparrow}, \quad (4)$$

with $V^{\text{II}} = V_{1\uparrow 1\downarrow 1\downarrow 2\uparrow}^{c c v c} = (V^{\text{AR}})^*$. The Coulomb coupling elements V^{II} and V^{AR} are taken to be real and are thus equal, $V^{\text{II}} = V^{\text{AR}} \equiv V$.

The theoretical description developed in this work is inherently non-Markovian and hence allows to study the dynamics including non-energy-conserving scattering processes. This will be utilized later to study the effect of off-resonant Coulomb scattering on the efficiency of the impact ionization process.

For our calculations, we assume that the coupling elements are determined by an ab initio theory such as in Ref. 15, thus focusing on the ultrafast time scale of the quantum-kinetic dynamics. The parameters are chosen for the PbSe QD of Ref. 9, yielding approximate values for the energetic and coupling parameters.

III. DYNAMICAL EQUATIONS

The quantum-kinetic dynamics is derived within an equation of motion approach.¹⁶ The finite character of the four-electron system is used to close the hierarchy of expectation values arising from the many-particle interaction Hamiltonian H_{Coul} , making the calculated results essentially non-perturbative with respect to the Coulomb interaction. The restriction to four electrons is a good assumption if the interaction between the electrons inside the quantum dot and the electrons of the surrounding substrate is negligibly weak.¹⁷ Within this assumption, all correlations containing ten or more electron operators vanish because they describe correlations between more than four electrons.

Since we focus on ultrashort time scales (subpicosecond), the influence of radiative decay on the carrier dynamics, which acts on comparably long time scales ($T_1 \geq 1$ ns) resulting from the small energy gaps, will be neglected throughout this work. However, pure dephasing processes are considered via a phenomenological constant γ_{PD} .

It turns out that for the system introduced in Sec. II including the impact ionization and Auger recombination of only the conduction band electrons, a reduction to a two-electron description yields results close to the full calculations involving all electron correlations. Therefore, to achieve greater clarity, we will use the two-electron level for a discussion of the system properties. The final dynamical results presented in the figures, however, are calculated using the full set of equations, cf. the appendix for the equations. We would like to note that an analogous set of dynamical equations was used in Ref. 9 to discuss the time dynamics of absorption bleaching in QDs.

To present a clear depiction of the processes and their mutual dependencies, the operator abbreviations used

are listed in table I.

Abbreviation	Operator
$f_{\lambda s}^c$	$a_{c\lambda s}^\dagger a_{c\lambda s}$
$f_{\lambda s}^v$	$a_{v\lambda s}^\dagger a_{v\lambda s}$
$p_{2\uparrow}$	$a_{c2\uparrow}^\dagger a_{v2\uparrow}$
p_{DE}	$a_{c1\uparrow}^\dagger a_{c1\downarrow}^\dagger a_{v1\downarrow} a_{v2\uparrow}$
p_{II}	$a_{c1\uparrow}^\dagger a_{c1\downarrow}^\dagger a_{v1\downarrow} a_{c2\uparrow}$

TABLE I: Operator abbreviations: $f_{\lambda s}^{c(v)}$ is the occupation operator in subband λ with spin s in the conduction (valence) band. $p_{2\uparrow}$ describes the transition of an electron from state $|v2\uparrow\rangle$ to $|c2\uparrow\rangle$ [cf. Fig. 1(b)]. The operator of the double excitation p_{DE} [cf. Fig. 1(e)] annihilates two electrons in the states $|v2\uparrow\rangle$ and $|v1\downarrow\rangle$ and creates two electrons in the states $|c1\uparrow\rangle$ and $|c1\downarrow\rangle$. The operator of impact ionization p_{II} [cf. Fig. 1(c)] describes the correlated transition between the states $|v1\downarrow\rangle$, $|c1\downarrow\rangle$ and the states $|c2\uparrow\rangle$, $|c1\uparrow\rangle$.

A. Energetic Structure and absorption of the QD

Before we investigate the full dynamics, we first characterize the electronic system via the linear optical absorption:

$$\alpha(\omega) \sim \omega \Im \left(\frac{P(\omega)}{\epsilon_0 E(\omega)} \right). \quad (5)$$

Since we are interested in the energetic structure of the system under excitation of the transition $|v2\uparrow\rangle \rightarrow |c2\uparrow\rangle$, we can restrict to the microscopic polarization $\langle p_{2\uparrow} \rangle$ [cf. table I], which determines the macroscopic polarization $P(t)$ via $P(t) \sim M_{2\uparrow}^{cv} \langle p_{2\uparrow} \rangle(t) + c.c.$

The system of dynamical equations defining the linear absorption $\alpha(\omega)$ via $\langle p_{2\uparrow} \rangle$ reads:

$$d_t \langle p_{2\uparrow} \rangle = \left[\frac{i}{\hbar} (\epsilon_{2\uparrow}^c - \epsilon_{2\uparrow}^v) - \gamma_{\text{PD}} \right] \langle p_{2\uparrow} \rangle + \frac{i}{\hbar} V \langle p_{\text{DE}} \rangle + \frac{i}{\hbar} E(t) M_{2\uparrow}^{cv}, \quad (6)$$

$$d_t \langle p_{\text{DE}} \rangle = \left\{ \frac{i}{\hbar} [(\epsilon_{1\uparrow}^c - \epsilon_{2\uparrow}^v) + (\epsilon_{1\downarrow}^c - \epsilon_{1\downarrow}^v)] - \gamma_{\text{PD}} \right\} \langle p_{\text{DE}} \rangle + \frac{i}{\hbar} V \langle p_{2\uparrow} \rangle. \quad (7)$$

The analytical solution of the absorption spectrum can be obtained via Fourier transformation, yielding

$$\alpha(\omega) \sim \Im \left(\frac{\omega |M_{2\uparrow}^{cv}|^2}{\Delta\epsilon - i\hbar\gamma_{\text{PD}} - \frac{V^2}{\hbar\omega - [(\epsilon_{1\uparrow}^c - \epsilon_{2\uparrow}^v) + (\epsilon_{1\downarrow}^c - \epsilon_{1\downarrow}^v)] - i\hbar\gamma_{\text{PD}}}} \right). \quad (8)$$

It can be seen that for a vanishing Coulomb coupling, the real part of the denominator vanishes for an energy

detuning $\Delta\epsilon = \hbar\omega - (\epsilon_{2\uparrow}^c - \epsilon_{2\uparrow}^v) = 0$ between the incident light field and the single-exciton energy $(\epsilon_{2\uparrow}^c - \epsilon_{2\uparrow}^v)$. For non-vanishing and sufficiently large Coulomb coupling, the detuning $\Delta = (\epsilon_{2\uparrow}^c - \epsilon_{2\uparrow}^v) - [(\epsilon_{1\uparrow}^c - \epsilon_{2\uparrow}^v) + (\epsilon_{1\downarrow}^c - \epsilon_{1\downarrow}^v)]$ between the energy of the single-exciton generated by the light field [Fig. 1(b)] $(\epsilon_{2\uparrow}^c - \epsilon_{2\uparrow}^v)$ and the energy of the two-exciton generated by the double excitation $\langle p_{\text{DE}} \rangle$ or impact ionization $\langle p_{\text{II}} \rangle$ [Fig. 1(c),(e)] $[(\epsilon_{1\uparrow}^c - \epsilon_{2\uparrow}^v) + (\epsilon_{1\downarrow}^c - \epsilon_{1\downarrow}^v)]$ dominates the root of the denominator and therefore the maxima of the absorption.

The linear absorption spectrum of the system for different coupling strengths V is shown in Fig. 2(a). The double peak structure is the consequence of the anticrossing as illustrated in Fig. 2(b) for different detunings Δ . The states are degenerate for vanishing Coulomb cou-

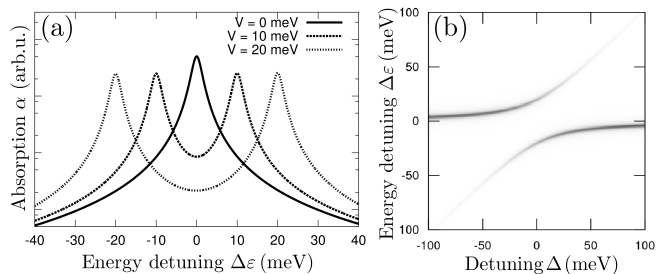


FIG. 2: (a) Linear absorption around the energy of the transition $|v2\uparrow\rangle \rightarrow |c2\uparrow\rangle$ for $\Delta = 0$ [energy-conserving impact ionization, cf. Fig. 1(c)] and different Coulomb coupling strengths V . (b) Linear absorption for $V = 20$ meV and varying detuning Δ and energy detuning $\Delta\epsilon$, showing an anticrossing between the single-exciton $|c2\uparrow v2\uparrow\rangle$ and two-exciton state $|c1\uparrow c1\downarrow v1\downarrow v2\uparrow\rangle$.

pling; for non-vanishing coupling, new eigenstates which are superpositions of the unperturbed states appear. In the following discussion, the system will be resonantly excited on the higher energetic branch [cf. Fig. 2(b)] except where explicitly noted otherwise. This excitation energy is found to be $\hbar\omega \approx (\epsilon_{2\uparrow}^c - \epsilon_{2\uparrow}^v + V)$ for $V \gtrsim 3$ meV in the case of a vanishing detuning Δ , which describes energy-conserving impact ionization as considered here, cf. Fig. 1(c).

B. Structure of the dynamics

Since the process of impact ionization is the focus of this study, we start the discussion of the dynamical structure with the expectation value $\langle p_{\text{II}} \rangle = \langle a_{c1\uparrow}^\dagger a_{c1\downarrow}^\dagger a_{v1\downarrow} a_{c2\uparrow} \rangle$ [cf. table I], which is the probability amplitude of the impact ionization process (generation of two electrons in the conduction band via one electron in

If the typical time scales \hbar/V and τ (pulse duration) of the two interactions V and $M(t)$ obey the relation $\tau \lesssim \hbar/V$, the dynamics can be divided into sequential interaction steps: For example, for a short light-matter (τ) and a comparably long Coulomb interaction time (\hbar/V), the dynamics is first restricted solely to the left contribution of path 1. For longer times, the right contribution of path 1 is activated by the non-vanishing density-density correlation $\langle f_{2\uparrow}^c f_{1\downarrow}^v \rangle$, while path 2 remains dormant due to vanishing intermittent polarizations. For a light-matter interaction strongly exceeding the Coulomb interaction time scale, i.e., $\tau \gg \hbar/V$, the dynamics is comprised of an interference of both paths.

A case where path 2 dominates the dynamics while path 1 remains dormant is not possible, as can be seen in Fig. 3. Let us assume that \hbar/V is negligible compared to τ . Even though $\langle p_{\text{DE}} \rangle$ of path 2 is then driven on a much shorter time scale than the density-density correlation $\langle f_{2\uparrow}^c f_{1\downarrow}^v \rangle$ of path 1 via the polarization $\langle p_{2\uparrow} f_{1\downarrow}^v \rangle$, this process is compensated by the slower time scale of the second step between $\langle p_{\text{DE}} \rangle$ and $\langle p_{\text{II}} \rangle$ as compared to the case for the density-density correlation $\langle f_{2\uparrow}^c f_{1\downarrow}^v \rangle$. Thus, no qualitative difference in the behavior is expected when taking the limiting case of $\tau \gg \hbar/V$, which is just due to the fact that the Coulomb interaction acts at all times.

We will come back to the dynamical structure via the two paths in the following sections to explain the numerical results.

IV. CARRIER MULTIPLICATION

We now turn to the central focus of the article, the investigation of the ultrafast dynamics of carrier multiplication. As a measure of the process, we define the carrier multiplication CM as the ratio of the total carrier occupation in the conduction band $\langle f_c \rangle$ and its light-induced part $\langle f_c \rangle|_{\text{light}}$, i.e., the conduction band carrier density which is excited solely by the light field:

$$\text{CM} = \frac{\langle f_c \rangle}{\langle f_c \rangle|_{\text{light}}} . \quad (15)$$

The quantity CM is equal to one if no *additional* carriers are created by the Coulomb coupling ($\langle f_c \rangle = \langle f_c \rangle|_{\text{light}}$). Its maximal value in the model system treated in this paper (cf. Sec. II) is 2. This results from the fact that the electronic excess energy is equal to two times the band gap energy. We will now derive the explicit expressions for the total carrier occupation in the conduction band $\langle f_c \rangle$, its Coulomb-induced part $\langle f_c \rangle|_{\text{Coul}}$ and its light-induced part $\langle f_c \rangle|_{\text{light}}$.

The total carrier occupation in the conduction band reads

$$\langle f_c \rangle = \sum_{\lambda,s} \langle a_{c\lambda s}^\dagger a_{c\lambda s} \rangle = \langle f_{2\uparrow}^c \rangle + \langle f_{1\uparrow}^c \rangle + \langle f_{1\downarrow}^c \rangle . \quad (16)$$

The occupation $\langle f_{2\downarrow}^c \rangle$ is neither driven by the external optical field nor by Coulomb scattering and therefore remains zero. Considering the dynamical equation for $\langle f_c \rangle$,

$$d_t \langle f_c \rangle = \underbrace{\frac{2}{\hbar} M(t) \Im(\langle p_{2\uparrow} \rangle_{-1})}_{d_t \langle f_c \rangle|_{\text{light}}} + \underbrace{\frac{2}{\hbar} V \Im(\langle p_{\text{II}} \rangle)}_{d_t \langle f_c \rangle|_{\text{Coul}}} , \quad (17)$$

two source terms $\langle f_c \rangle|_{\text{light}}$ and $\langle f_c \rangle|_{\text{Coul}}$ can be identified, relating to the light-matter coupling $M(t)$ and the impact ionization transition probability, respectively. Thus, the carrier multiplication CM can be computed.

In the following, we analyze carrier multiplication for both the energy-conserving and the non-energy-conserving case numerically, using the parameters in table II if not noted otherwise.

Parameter	Value
$\epsilon_{2\uparrow}^v, \epsilon_{2\downarrow}^v$	-400 meV
$\epsilon_{1\uparrow}^v, \epsilon_{1\downarrow}^v$	0 meV
$\epsilon_{1\uparrow}^c, \epsilon_{1\downarrow}^c$	400 meV
$\epsilon_{2\uparrow}^c, \epsilon_{2\downarrow}^c$	800 meV
V	20 meV
γ_{PD}	1/(500 fs)

TABLE II: The electronic energy structure and the Coulomb coupling elements are taken from Ref. 9 for a PbSe quantum dot of diameter $d = 5$ nm. This system provides a small band gap and allows energy conserving impact ionization and Auger recombination processes.

A. General Properties of our Model

We first discuss the general relation between the total carrier occupation and its light- and Coulomb-induced parts in our model system. This will be useful in understanding the dynamical behavior of these quantities in the next section.

The inversion driving the impact ionization [cf. Eq. 9] and Auger recombination can be expressed in terms of the light- and Coulomb-induced parts of the total carrier occupation:

$$\langle f_{2\uparrow}^c f_{1\downarrow}^v \rangle - \langle f_{1\uparrow}^c f_{1\downarrow}^c \rangle = \langle f_c \rangle|_{\text{light}} - 2\langle f_c \rangle|_{\text{Coul}} . \quad (18)$$

Here, we employed the dynamical equations (11,12) and the definitions of $\langle f_c \rangle|_{\text{light}}$ and $\langle f_c \rangle|_{\text{Coul}}$ as well as their initial values. For a vanishing inversion, the ratio of $\langle f_c \rangle|_{\text{Coul}}$ and $\langle f_c \rangle|_{\text{light}}$ is obtained as

$$\langle f_c \rangle|_{\text{Coul}} = 1/2 \langle f_c \rangle|_{\text{light}} . \quad (19)$$

This is equivalent to a carrier multiplication CM = 1.5, which is reached in a quasi-stationary limit, where all

polarizations (in particular, the impact ionization and Auger recombination amplitudes) vanish.

In our model system, this value is obtained on long time scales independent of the exciting pulse parameters, as will be seen in the next sections. This is due to the fact that we do not include relaxation effects such as phonon-assisted intraband relaxation, since we want to focus on the ultrafast time dynamics of carrier multiplication. Furthermore, we will see that, in contrast to first expectations, reaching this quasi-stationary state of the system does *not* solely depend on the damping of the participating polarizations by pure-dephasing processes, but can be reached on an ultrafast timescale by control of the pulse duration τ .

A complementary analysis was performed in Ref. 9 for the absorption bleaching, focusing on the relation between the Coulomb interaction strength and the relaxation rates of the single-exciton and two-exciton states. Here, we focus on the relation of the Coulomb coupling strength to the externally controllable pulse length, allowing an external control in the detection of carrier multiplication. Since we do not consider relaxation processes, we are thus in the regime where oscillations are observed in the absorption bleaching in Ref. 9.

B. Energy-Conserving Case

We begin our investigation of the dynamics by considering energy-conserving impact ionization, i.e., we assume the energetic structure given in table II, where $\epsilon_{2\uparrow}^c - \epsilon_{1\uparrow}^c = \epsilon_{1\downarrow}^c - \epsilon_{1\downarrow}^v$. We differentiate between two different regimes: (i) the light-matter coupling occurs on a shorter time scale than the Coulomb coupling, i.e., the pulse duration τ is shorter than the typical Coulomb interaction time (\hbar/V), $\tau \lesssim \hbar/V$ and (ii) the light-matter coupling strongly exceeds the Coulomb coupling, $\tau \gg \hbar/V$.

(i) $\tau \lesssim \hbar/V$: Figure 4(a) shows the conduction band carrier occupation $\langle f_c \rangle$ and the contribution from the light-matter interaction $\langle f_c \rangle|_{\text{light}}$ for an excitation with a 20 fs pulse with a pulse area of 0.1π . The light pulse induces a density in the conduction band $\langle f_c \rangle|_{\text{light}}$ at $t \approx 0$ ps. After the pulse, $\langle f_c \rangle|_{\text{light}}$ remains constant (dashed line) and is exceeded by the total carrier density (solid line) $\langle f_c \rangle$, which indicates carrier multiplication. $\langle f_c \rangle$ exhibits clear oscillations above the level of $\langle f_c \rangle|_{\text{light}}$.

As discussed in Sec. III B, the build-up of the light- and Coulomb-induced carrier density occurs *sequentially* via path 1 depicted in Fig. 3. For the considered parameter range, on a short time scale, determined by the light-matter interaction τ , the light field induces the density-density correlation $\langle f_{2\uparrow}^c f_{1\downarrow}^v \rangle$ which, on a time scale determined by the Coulomb coupling \hbar/V , creates the density-density correlation $\langle f_{1\uparrow}^c f_{1\downarrow}^c \rangle$ via impact ionization. During this build-up, impact ionization becomes increasingly inhibited because the inversion between the

density-density correlations $\langle f_{1\uparrow}^c f_{1\downarrow}^c \rangle$ and $\langle f_{2\uparrow}^c f_{1\downarrow}^v \rangle$ tends to zero, leading to a slowdown of impact ionization until a first maximum of $\langle f_c \rangle$ is reached, i.e., a state which favors Auger recombination over impact ionization. This leads to a subsequent decrease of the total carrier occupation towards a local temporal minimum until impact ionization starts to dominate again. The damping of the resulting oscillation of the total carrier occupation $\langle f_c \rangle$ is determined solely by the pure dephasing of the system.

The basic physical picture of the oscillation is the anticrossing described in Sec. III B: The spectrally broad pulse simultaneously excites both eigenstates, creating an inversion between the unperturbed states, i.e., between the correlations $\langle f_{2\uparrow}^c f_{1\downarrow}^v \rangle$ and $\langle f_{1\uparrow}^c f_{1\downarrow}^c \rangle$ [cf. Eq. (9)]. The limit of CM = 1.5 is reached as soon as the pure dephasing has damped the participating polarizations.

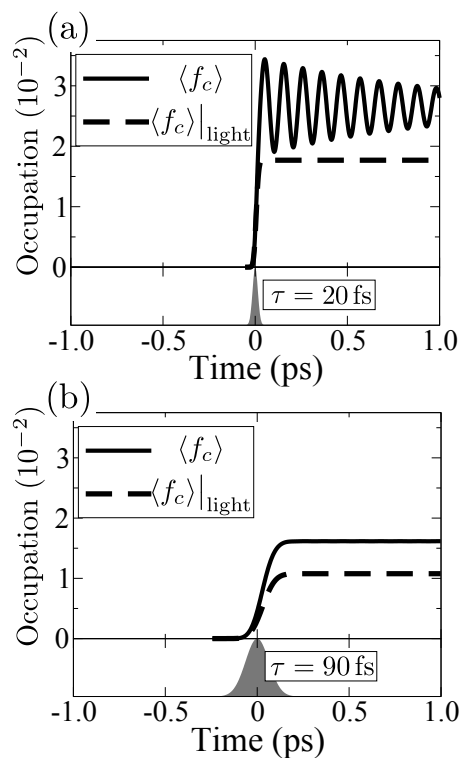


FIG. 4: Dynamics of the conduction band carrier occupation $\langle f_c \rangle$ and the contribution due to the light field $\langle f_c \rangle|_{\text{light}}$ for a pulsed excitation with a pulse area of 0.1π and pulse length of (a) $\tau = 20$ fs and (b) $\tau = 90$ fs.

(ii) $\tau \gg \hbar/V$: Under excitation with a longer light pulse ($\tau = 90$ fs), the time scale of the light-matter coupling strongly exceeds the Coulomb interaction ($\tau = 90$ fs, $\hbar/V \approx 35$ fs). This prevents carrier multiplication, i.e., the creation of the density-density correlation $\langle f_{1\uparrow}^c f_{1\downarrow}^c \rangle$, to occur as a sequential process of initial light excitation and following impact ionization alone. Now, the paths depicted in Fig. 3 describing a sequential (path 1) and a simultaneous (path 2) creation of the density-density correlation $\langle f_{1\uparrow}^c f_{1\downarrow}^c \rangle$ contribute both and lead to

a concurrent growth of the light-induced $\langle f_c \rangle|_{\text{light}}$ and Coulomb-induced $\langle f_c \rangle|_{\text{Coul}}$ carrier densities in the conduction band. Figure 4(b) shows that carrier multiplication still occurs, even though no oscillations (no subsequent impact ionization and Auger recombination) are found in the total carrier density $\langle f_c \rangle$. This is due to a balance between the densities driving the impact ionization, and therefore a vanishing inversion, resulting from the interplay of paths 1 and 2. This balance causes the carrier multiplication limit of $\text{CM} = 1.5$ to be reached nearly simultaneously with the exciting light pulse on a much shorter timescale than in the case of short pulse excitation.

C. Non-energy-conserving Case

When the Coulomb-coupled single-exciton and two-exciton states are off-resonant, i.e., $\epsilon_{2\uparrow}^c - \epsilon_{1\uparrow}^c \neq \epsilon_{1\downarrow}^c - \epsilon_{1\downarrow}^v$, the influence of impact ionization is strongly suppressed, because energy conservation is violated by this scattering process. To investigate this quantitatively for our Coulomb parameters (cf. table II), the time evolution of the conduction band densities $\langle f_c \rangle$ and $\langle f_c \rangle|_{\text{light}}$ is shown in Fig. 5(a) for an exemplary detuning $\Delta = 100$ meV between the Coulomb-coupled states and a pulse length of 20 fs. The detuning Δ is achieved by varying the energy $\epsilon_{1\downarrow}^v$, while the other parameters remain fixed. The system is excited resonantly on the single-exciton energy $\epsilon_{2\uparrow}^c - \epsilon_{2\uparrow}^v$.

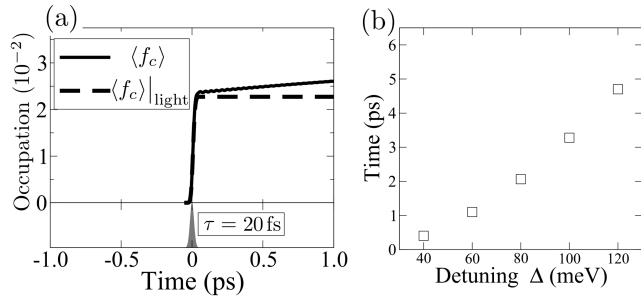


FIG. 5: (a) Time evolution of the total carrier occupation in the conduction band $\langle f_c \rangle$ and its light-induced part $\langle f_c \rangle|_{\text{light}}$ for a detuning of $\Delta = 100$ meV between the Coulomb-coupled states and an excitation with a 20 fs, 0.1π pulse. (b) Impact ionization times, defined as the time of the system to reach a carrier multiplication factor of $\text{CM} = 1.316 (= 1 + 0.5(1 - e^{-1}))$ over the detuning $|\Delta|$ for an excitation resonant on the single-exciton energy $\hbar\omega_L = (\epsilon_{2\uparrow}^c - \epsilon_{2\uparrow}^v)$.

The Coulomb-induced conduction band density $\langle f_c \rangle|_{\text{Coul}}$, and thus the process of carrier multiplication, is negligibly weak on an ultrafast subpicosecond time scale. For very long time scales, the CM again approaches 1.5, as discussed in Sec. IV A, assuming that no radiative recombination and phonon-assisted intraband relaxation are considered. However, when these processes are con-

sidered, which act on a picosecond time scale in the case of phonon-assisted relaxation, the carrier multiplication will dramatically decrease below $\text{CM} = 1.5$.

To investigate the influence of off-resonant Coulomb scattering processes on the timescale of carrier multiplication, we plot the time in which a value $\text{CM} = 1.316$, corresponding to the exponential growth value of the CM maximum, is reached over the detuning Δ in Fig. 5(b). Carrier multiplication times of a few picoseconds, which lie in the range of typical phonon-assisted relaxation times,¹⁸ occur for a detuning $\Delta \gtrsim 100$ meV.

Thus, for sufficient detuning between the Coulomb-coupled states, impact ionization is expected to be negligible. This result can also be used to justify neglecting impact ionization scattering in the valence band in material systems which show a large difference in the effective masses in the conduction and valence band. Nevertheless, it should be noted that this result is crucially dependent on the Coulomb coupling strength V . A stronger coupling would raise the importance of non-energy-conserving impact ionization for a given detuning Δ .

D. Inclusion of valence band impact ionization

To include the influence of impact ionization and Auger recombination in the valence band [Fig. 1(d)] in our dynamics, we generalize the Coulomb Hamiltonian H_{Coul} :

$$H_{\text{Coul}} = V^{\text{II}} a_{c1\uparrow}^\dagger a_{c1\downarrow}^\dagger a_{v1\downarrow} a_{c2\uparrow} + V^{\text{AR}} a_{c2\uparrow}^\dagger a_{v1\downarrow}^\dagger a_{c1\downarrow} a_{c1\uparrow} \\ + \bar{V}^{\text{II}} a_{v2\uparrow}^\dagger a_{c1\downarrow}^\dagger a_{v1\downarrow} a_{v1\uparrow} + \bar{V}^{\text{AR}} a_{v1\uparrow}^\dagger a_{v1\downarrow}^\dagger a_{c1\downarrow} a_{v2\uparrow},$$

with the coupling elements $\bar{V}^{\text{II}} = V_{2\uparrow 1\downarrow 1\downarrow 1\uparrow}^{v c v v} = (\bar{V}^{\text{AR}})^*$. This introduces additional valence band scattering correlations as well as correlations linking both bands.

Figure 6 shows the corresponding dynamics with $(\langle f_c \rangle|_{C+V})$ and without $(\langle f_c \rangle|_C)$ impact ionization of valence band electrons for a short pulse excitation. The system is again excited resonant on the higher energetic branch, and the conduction and valence band impact ionization coupling elements are taken to be equal, $V = \bar{V} = 20$ meV. The occurring oscillation describing impact ionization and Auger recombination has a higher frequency for the inclusion of both processes which corresponds to a larger effective Coulomb coupling $V_{\text{eff}}(V, \bar{V})$. For the long pulse excitation, no significant differences are found.

V. TIME-RESOLVED OPTICAL EMISSION

In a next step, we investigate the obtained dynamical results in the time-resolved optical emission of the quantum dot during the impact ionization process, opening an alternative approach to measure MEG. In order to describe this quantum-optical signal, we consider the fully

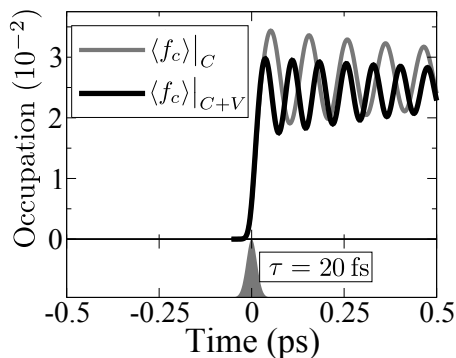


FIG. 6: Time evolution of the total carrier occupation in the conduction band with $\langle f_c \rangle_{C+V}$ and without $\langle f_c \rangle_C$ impact ionization processes in the valence band. The system is again excited on the higher energetic branch. Differences between the oscillation frequencies and the mean values of the total occupation $\langle f_c \rangle$ result from a changed effective Coulomb coupling constant.

quantized light-matter interaction Hamiltonian

$$H_{\text{QO}} = \sum_{\mathbf{k}} M_{2\uparrow}^{\mathbf{k}} a_{c2\uparrow}^{\dagger} a_{v2\uparrow} c_{\mathbf{k}} + \text{h.a.}, \quad (20)$$

with the electron-photon coupling element $M_{2\uparrow}^{\mathbf{k}} = i\sqrt{\frac{\hbar\omega_{\mathbf{k}}}{2\epsilon_0 V}} M_{2\uparrow}^{cv}$ in dipole approximation; $c_{\mathbf{k}}^{(\dagger)}$ is the photonic annihilation (creation) operator in mode \mathbf{k} . Analogous to the consideration of the semiclassical light-matter interaction, a rotating-wave approximation is applied on the frequency of the external excitation. The hierarchy of dynamical equations stemming from the electron-photon interaction is truncated on the two-photon level, i.e., two-photon assisted electronic correlations are neglected.

The time-resolved emission spectrum at an observation frequency $\omega_{\mathbf{k}_s}$ at a distance z to the detector is given by¹⁹

$$S(z\vec{e}_z, \omega_{\mathbf{k}_s}, t) = \sum_{\mathbf{k}_1, \mathbf{k}_2} \frac{\hbar\sqrt{\omega_{\mathbf{k}_1}\omega_{\mathbf{k}_2}}}{2\epsilon_0 c^2 \Omega} \langle c_{\mathbf{k}_1}^{\dagger} c_{\mathbf{k}_2} \rangle e^{-i(k_1 - k_2)z} \times e^{-[(k_1 - k_s)c\Delta t/\sqrt{2}]^2} e^{-[(k_2 - k_s)c\Delta t/\sqrt{2}]^2}, \quad (21)$$

with the time uncertainty of the detector Δt , the quantization volume Ω , the speed of light c , and the vacuum dielectric constant ϵ_0 . The angular frequencies ω_i and the momenta k_i are related via the linear dispersion relation $\omega_i = ck_i$. The time uncertainty Δt has to be equal to or smaller than the pulse length τ in order to resolve the time evolution of the exciting light pulse.

In Figs. 7(a-c), the resulting time-resolved emission spectrum is shown for increasing pulse lengths $\tau = 20$ fs, 40 fs, and 90 fs. The time uncertainty Δt is set to 20 fs in order to resolve the temporal dynamics. In the calculations, the full system including impact ionization and Auger recombination in both the conduction and valence band is considered. For a short pulse excitation

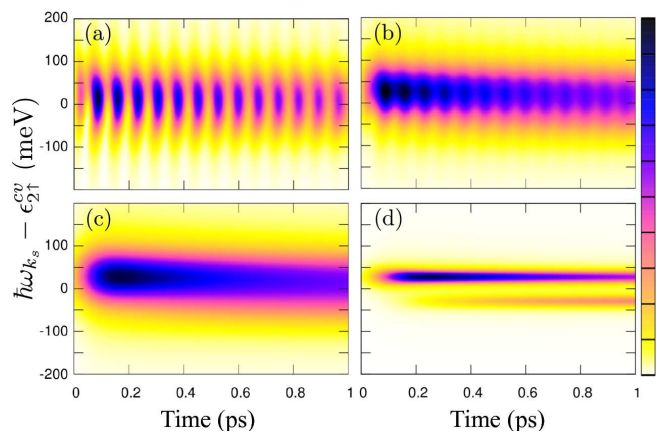


FIG. 7: (Color online) Time-resolved optical emission spectra around the energy of the single-exciton $\epsilon_{2\uparrow}^{cv} = (\epsilon_{2\uparrow}^c - \epsilon_{2\uparrow}^v)$ for an excitation with a pulse area of 0.1π and pulse length (a) $\tau = 20$ fs, (b) $\tau = 40$ fs, and (c),(d) $\tau = 90$ fs. (a)-(c) The time uncertainty of the detector is set to $\Delta t = 20$ fs. A transition from oscillating to non-oscillating behavior occurs, corresponding to the carrier dynamics discussed earlier. (d) For a larger time uncertainty $\Delta t = 20$ fs, the better energetic resolution reveals the substructure of the fluorescence corresponding to the observed anticrossing in the linear absorption.

[Fig. 7(a)], oscillations in the emission are found, corresponding to the impact ionization-induced carrier dynamics in Fig. 4(a). These oscillations become less pronounced for an intermediate pulse length [Fig. 7(b)] and disappear for an excitation with a long pulse [Fig. 7(c)]. Thus, the quantum-kinetic signatures, resulting from the interplay between the light-matter and the Coulomb interaction, are recovered directly in the time-resolved optical emission.

To recover the energetic structure of the QD, the time uncertainty of the detector is increased in Fig. 7(d) to allow for a sufficient energetic resolution. The observed energetic splitting of the fluorescence line corresponds to the anticrossing in the linear absorption (cf. Fig. 2). The earlier onset of the signal at the energetically higher branch results from the Rayleigh signal of the exciting light pulse.

VI. CONCLUSION

A quantum-kinetic approach to the dynamics of carrier multiplication in quantum dots was presented, focusing on the interplay between the light-matter and the Coulomb interaction on ultrafast timescales, where intraband relaxation is of minor importance. The analysis of the underlying dynamics revealed two different paths leading to multiple carriers in the conduction band, controllable via the coupling parameters of the two interactions: the duration of the exciting light pulse and the Coulomb interaction time.

We observe the occurrence of oscillations for certain ex-

ternally controllable excitation parameters. These oscillations result from the interplay of impact ionization and Auger recombination and could in principle be used to detect carrier multiplication before relaxation processes occur. The corresponding distinct signatures in the time-resolved optical emission spectrum open the possibility for an alternative approach to measure multi-exciton generation in quantum dots. In particular, they might offer the possibility to distinguish carrier multiplication in quantum dots by Auger-type processes from other processes, such as multiphoton excitation, uncontrolled photocharging, and influences of the surface chemistry, which can lead to ambiguities in the analysis of excitonic decay dynamics.^{5,6,20}

It was also shown that the time dynamics does not qualitatively change when neglecting impact ionization scattering in the valence band, resulting only in small modifications in the carrier occupations. Furthermore, the investigation of non-energy-conserving impact ionization and Auger recombination highlights how crucial resonance is for the impact ionization process.

1. Electronic system

As in Sec. III B, we begin with the dynamical equation of the impact ionization amplitude:

$$\begin{aligned} d_t \langle p_{\text{II}} \rangle &= \frac{i}{\hbar} (\epsilon_{1\uparrow}^c + \epsilon_{1\downarrow}^c - \epsilon_{1\downarrow}^v - \epsilon_{2\uparrow}^c + i\hbar\gamma_{\text{PD}}) \langle p_{\text{II}} \rangle \\ &\quad - \frac{i}{\hbar} M(t) \langle p_{\text{DE}} \rangle_{-1} + \frac{i}{\hbar} V \langle f_{2\uparrow}^c f_{1\uparrow}^c f_{1\downarrow}^c \rangle \\ &\quad + \frac{i}{\hbar} V (\langle f_{2\uparrow}^c f_{1\downarrow}^v \rangle - \langle f_{1\uparrow}^c f_{1\downarrow}^c \rangle) \\ &\quad - \frac{i}{\hbar} V (\langle f_{2\uparrow}^c f_{1\uparrow}^c f_{1\downarrow}^v \rangle + \langle f_{2\uparrow}^c f_{1\downarrow}^c f_{1\downarrow}^v \rangle) \end{aligned} \quad (\text{A.1})$$

Next, we continue with the two-electron correlations:

$$\begin{aligned} d_t \langle p_{\text{DE}} \rangle_{-1} &= \frac{i}{\hbar} (\epsilon_{1\uparrow}^c + \epsilon_{1\downarrow}^c - \epsilon_{1\downarrow}^v - \epsilon_{2\uparrow}^v - \hbar\omega_L + i\hbar\gamma_{\text{PD}}) \langle p_{\text{DE}} \rangle_{-1} \\ &\quad - \frac{i}{\hbar} M(t) \langle p_{\text{II}} \rangle + \frac{i}{\hbar} V \langle f_{1\downarrow}^v p_{2\uparrow} \rangle_{-1} \\ &\quad + \frac{i}{\hbar} V (\langle f_{1\uparrow}^c f_{1\downarrow}^c p_{2\uparrow} \rangle_{-1} - \langle f_{1\downarrow}^c f_{1\uparrow}^v p_{2\uparrow} \rangle_{-1}) \\ &\quad - \frac{i}{\hbar} V \langle f_{1\uparrow}^c f_{1\downarrow}^v p_{2\uparrow} \rangle_{-1} \end{aligned} \quad (\text{A.2})$$

$$d_t \langle f_{2\uparrow}^c f_{1\downarrow}^v \rangle = \frac{2}{\hbar} M(t) \Im(\langle f_{1\downarrow}^v p_{2\uparrow} \rangle_{-1}) - \frac{2}{\hbar} V \Im(\langle p_{\text{II}} \rangle) \quad (\text{A.3})$$

$$d_t \langle f_{1\uparrow}^c f_{1\downarrow}^c \rangle = \frac{2}{\hbar} V \Im(\langle p_{\text{II}} \rangle) \quad (\text{A.4})$$

$$\begin{aligned} d_t \langle f_{1\downarrow}^v p_{2\uparrow} \rangle_{-1} &= \frac{i}{\hbar} (\epsilon_{2\uparrow}^c - \epsilon_{2\uparrow}^v - \hbar\omega_L + i\hbar\gamma_{\text{PD}}) \langle f_{1\downarrow}^v p_{2\uparrow} \rangle_{-1} \\ &\quad + \frac{i}{\hbar} V (\langle p_{\text{DE}} \rangle_{-1} - \langle f_{2\uparrow}^c p_{\text{DE}} \rangle_{-1}) \\ &\quad + \frac{i}{\hbar} M(t) (\langle f_{2\uparrow}^v f_{1\downarrow}^v \rangle - \langle f_{2\uparrow}^c f_{1\downarrow}^c \rangle) \end{aligned} \quad (\text{A.5})$$

$$d_t \langle f_{2\uparrow}^v f_{1\downarrow}^v \rangle = -\frac{2}{\hbar} M(t) \Im(\langle f_{1\downarrow}^v p_{2\uparrow} \rangle_{-1}) - \frac{2}{\hbar} V \Im(\langle f_{2\uparrow}^v p_{\text{II}} \rangle) \quad (\text{A.6})$$

Acknowledgments

We acknowledge financial support by the Deutsche Forschungsgemeinschaft via GRK1558 "Nonequilibrium Collective Dynamics in Condensed Matter and Biological Systems".

Appendix: Dynamical equations

In the following, we present the dynamical equations used in the calculations. We restrict the equations to impact ionization and Auger recombination processes in the conduction band.

The equations necessary to define the total carrier occupation and its parts are:

$$\begin{aligned} d_t \langle p_{2\uparrow} \rangle_{-1} &= \frac{i}{\hbar} (\epsilon_{2\uparrow}^c - \epsilon_{2\uparrow}^v - \hbar\omega_L + i\hbar\gamma_{\text{PD}}) \langle p_{2\uparrow} \rangle_{-1} \quad (\text{A.7}) \\ &\quad + \frac{i}{\hbar} M(t) (\langle f_{2\uparrow}^v \rangle - \langle f_{2\uparrow}^c \rangle) + \frac{i}{\hbar} V \langle p_{\text{DE}} \rangle_{-1} \end{aligned}$$

$$d_t \langle f_{2\uparrow}^v \rangle = -\frac{2}{\hbar} M(t) \Im(\langle p_{2\uparrow} \rangle_{-1}) \quad (\text{A.8})$$

$$d_t \langle f_{2\uparrow}^c \rangle = \frac{2}{\hbar} M(t) \Im(\langle p_{2\uparrow} \rangle_{-1}) - \frac{2}{\hbar} V \Im(\langle p_{\text{II}} \rangle) \quad (\text{A.9})$$

$$d_t \langle f_{1\uparrow}^c \rangle = \frac{2}{\hbar} V \Im(\langle p_{\text{II}} \rangle) \quad (\text{A.10})$$

$$d_t \langle f_{1\downarrow}^c \rangle = \frac{2}{\hbar} V \Im(\langle p_{\text{II}} \rangle) \quad (\text{A.11})$$

$$\begin{aligned} d_t \langle f_{1\uparrow}^c f_{1\downarrow}^c p_{2\uparrow} \rangle_{-1} &= \frac{i}{\hbar} V \langle f_{2\uparrow}^c p_{\text{DE}} \rangle_{-1} \\ &+ \frac{i}{\hbar} M(t) (\langle f_{1\uparrow}^c f_{1\downarrow}^c f_{2\uparrow}^v \rangle - \langle f_{2\uparrow}^c f_{1\uparrow}^c f_{1\downarrow}^c \rangle) \\ &+ \frac{i}{\hbar} (\epsilon_{2\uparrow}^c - \epsilon_{2\uparrow}^v - \hbar\omega_L + i\hbar\gamma_{\text{PD}}) \langle f_{1\uparrow}^c f_{1\downarrow}^c p_{2\uparrow} \rangle_{-1} \end{aligned} \quad (\text{A.12})$$

Finally, the dynamical equations for all higher correlations are given by

$$\begin{aligned} d_t \langle f_{1\downarrow}^c f_{1\downarrow}^v p_{2\uparrow} \rangle_{-1} &= \frac{i}{\hbar} M(t) (\langle f_{1\downarrow}^c f_{2\uparrow}^v f_{1\downarrow}^v \rangle - \langle f_{2\uparrow}^c f_{1\downarrow}^c f_{1\downarrow}^v \rangle) \\ &+ \frac{i}{\hbar} (\epsilon_{2\uparrow}^c - \epsilon_{2\uparrow}^v - \hbar\omega_L + i\hbar\gamma_{\text{PD}}) \langle f_{1\downarrow}^c f_{1\downarrow}^v p_{2\uparrow} \rangle_{-1} \end{aligned} \quad (\text{A.13})$$

$$\begin{aligned} d_t \langle f_{1\uparrow}^c f_{1\downarrow}^v p_{2\uparrow} \rangle_{-1} &= \frac{i}{\hbar} M(t) (\langle f_{1\uparrow}^c f_{2\uparrow}^v f_{1\downarrow}^v \rangle - \langle f_{2\uparrow}^c f_{1\uparrow}^c f_{1\downarrow}^v \rangle) \\ &+ \frac{i}{\hbar} (\epsilon_{2\uparrow}^c - \epsilon_{2\uparrow}^v - \hbar\omega_L + i\hbar\gamma_{\text{PD}}) \langle f_{1\uparrow}^c f_{1\downarrow}^v p_{2\uparrow} \rangle_{-1} \end{aligned} \quad (\text{A.14})$$

$$d_t \langle f_{2\uparrow}^c f_{1\downarrow}^c f_{1\downarrow}^v \rangle = \frac{2}{\hbar} M(t) \Im(\langle f_{1\downarrow}^c f_{1\downarrow}^v p_{2\uparrow} \rangle_{-1}) \quad (\text{A.15})$$

$$d_t \langle f_{2\uparrow}^c f_{1\uparrow}^c f_{1\downarrow}^c \rangle = \frac{2}{\hbar} M(t) \Im(\langle f_{1\uparrow}^c f_{1\downarrow}^c p_{2\uparrow} \rangle_{-1}) \quad (\text{A.16})$$

$$d_t \langle f_{2\uparrow}^c f_{1\uparrow}^c f_{1\downarrow}^v \rangle = \frac{2}{\hbar} M(t) \Im(\langle f_{1\uparrow}^c f_{1\downarrow}^v p_{2\uparrow} \rangle_{-1}) \quad (\text{A.17})$$

$$\begin{aligned} d_t \langle f_{2\uparrow}^c p_{\text{DE}} \rangle_{-1} &= -\frac{i}{\hbar} M(t) \langle f_{2\uparrow}^c p_{\text{II}} \rangle + \frac{i}{\hbar} V \langle f_{1\uparrow}^c f_{1\downarrow}^c p_{2\uparrow} \rangle_{-1} \\ &+ \frac{i}{\hbar} (\epsilon_{1\uparrow}^c + \epsilon_{1\downarrow}^c - \epsilon_{1\downarrow}^v - \epsilon_{2\uparrow}^v - \hbar\omega_L + i\gamma_{\text{PD}}\hbar) \langle f_{2\uparrow}^c p_{\text{DE}} \rangle_{-1} \end{aligned} \quad (\text{A.18})$$

$$\begin{aligned} d_t \langle f_{1\uparrow}^c f_{1\downarrow}^c f_{2\uparrow}^v \rangle &= -\frac{2}{\hbar} M(t) \Im(\langle f_{1\uparrow}^c f_{1\downarrow}^c p_{2\uparrow} \rangle_{-1}) \\ &+ \frac{2}{\hbar} V \Im(\langle f_{2\uparrow}^c p_{\text{II}} \rangle) \end{aligned} \quad (\text{A.19})$$

$$d_t \langle f_{1\downarrow}^c f_{2\uparrow}^v f_{1\downarrow}^v \rangle = -\frac{2}{\hbar} M(t) \Im(\langle f_{1\downarrow}^c f_{1\downarrow}^v p_{2\uparrow} \rangle_{-1}) \quad (\text{A.20})$$

$$d_t \langle f_{1\uparrow}^c f_{2\uparrow}^v f_{1\downarrow}^v \rangle = -\frac{2}{\hbar} M(t) \Im(\langle f_{1\uparrow}^c f_{1\downarrow}^v p_{2\uparrow} \rangle_{-1}) \quad (\text{A.21})$$

$$\begin{aligned} d_t \langle f_{2\uparrow}^v p_{\text{II}} \rangle &= -\frac{i}{\hbar} M(t) \langle f_{2\uparrow}^c p_{\text{DE}} \rangle_{-1} \\ &+ \frac{i}{\hbar} V (\langle f_{2\uparrow}^c f_{2\uparrow}^v f_{1\downarrow}^v \rangle - \langle f_{1\uparrow}^c f_{1\downarrow}^c f_{2\uparrow}^v \rangle) \\ &+ \frac{i}{\hbar} (\epsilon_{1\uparrow}^c + \epsilon_{1\downarrow}^c - \epsilon_{1\downarrow}^v - \epsilon_{2\uparrow}^c + i\gamma_{\text{PD}}\hbar) \langle f_{2\uparrow}^c p_{\text{II}} \rangle \end{aligned} \quad (\text{A.22})$$

$$d_t \langle f_{2\uparrow}^c f_{2\uparrow}^v f_{1\downarrow}^v \rangle = -\frac{2}{\hbar} V \Im(\langle f_{2\uparrow}^c p_{\text{II}} \rangle) \quad (\text{A.23})$$

The higher electronic correlations which are not driven are not displayed here.

2. Quantum-optical system

Next, we show the photon-assisted correlations, again restricting to the impact ionization and Auger recombination processes in the conduction band.

$$\begin{aligned} d_t \langle c_{\mathbf{k}2}^\dagger c_{\mathbf{k}1} \rangle &= \frac{i}{\hbar} M_{2\uparrow}^{\mathbf{k}} \langle p_{2\uparrow} c_{\mathbf{k}1} \rangle - \frac{i}{\hbar} M_{2\uparrow}^{\mathbf{k}*} \langle p_{2\uparrow}^\dagger c_{\mathbf{k}2}^\dagger \rangle \\ &+ \frac{i}{\hbar} (\hbar\omega_{\mathbf{k}2} - \hbar\omega_{\mathbf{k}1}) \langle c_{\mathbf{k}2}^\dagger c_{\mathbf{k}1} \rangle \end{aligned} \quad (\text{A.24})$$

$$\begin{aligned} d_t \langle p_{2\uparrow} c_{\mathbf{k}1} \rangle &= \frac{i}{\hbar} M(t) \langle f_{2\uparrow}^v c_{\mathbf{k}1} \rangle_{+1} - \frac{i}{\hbar} M(t) \langle f_{2\uparrow}^c c_{\mathbf{k}1} \rangle_{+1} \\ &+ \frac{i}{\hbar} V \langle p_{\text{DE}} c_{\mathbf{k}1} \rangle - \frac{i}{\hbar} M_{2\uparrow}^{\mathbf{k}*} \langle f_{2\uparrow}^c \rangle + \frac{i}{\hbar} M_{2\uparrow}^{\mathbf{k}*} \langle f_{2\uparrow}^c f_{2\uparrow}^v \rangle \\ &+ \frac{i}{\hbar} (\epsilon_{2\uparrow}^c - \epsilon_{2\uparrow}^v - \hbar\omega_{\mathbf{k}1} + i\gamma_{\text{PD}}\hbar) \langle p_{2\uparrow} c_{\mathbf{k}1} \rangle \end{aligned} \quad (\text{A.25})$$

$$\begin{aligned} d_t \langle f_{2\uparrow}^v c_{\mathbf{k}1} \rangle_{+1} &= \frac{i}{\hbar} M(t) (\langle p_{2\uparrow} c_{\mathbf{k}1} \rangle - \langle p_{2\uparrow}^\dagger c_{\mathbf{k}1} \rangle_{+2}) \\ &- \frac{i}{\hbar} M_{2\uparrow}^{\mathbf{k}*} \langle p_{2\uparrow}^\dagger \rangle_{+1} + \frac{i}{\hbar} (-\hbar\omega_{\mathbf{k}1} + \omega_L) \langle f_{2\uparrow}^v c_{\mathbf{k}1} \rangle_{+1} \end{aligned} \quad (\text{A.26})$$

$$\begin{aligned} d_t \langle f_{2\uparrow}^c c_{\mathbf{k}1} \rangle_{+1} &= \frac{i}{\hbar} M(t) (\langle p_{2\uparrow}^\dagger c_{\mathbf{k}1} \rangle_{+2} - \langle p_{2\uparrow} c_{\mathbf{k}1} \rangle) \\ &+ \frac{i}{\hbar} V \langle p_{\text{II}} c_{\mathbf{k}1} \rangle_{+1} - \frac{i}{\hbar} V \langle p_{\text{II}}^\dagger c_{\mathbf{k}1} \rangle_{+1} \\ &+ \frac{i}{\hbar} (-\hbar\omega_{\mathbf{k}1} + \omega_L) \langle f_{2\uparrow}^c c_{\mathbf{k}1} \rangle_{+1} \end{aligned} \quad (\text{A.27})$$

$$\begin{aligned} d_t \langle p_{2\uparrow}^\dagger c_{\mathbf{k}1} \rangle_{+2} &= -\frac{i}{\hbar} V \langle p_{\text{DE}}^\dagger c_{\mathbf{k}1} \rangle_{+2} \\ &+ \frac{i}{\hbar} M(t) \langle f_{2\uparrow}^c c_{\mathbf{k}1} \rangle_{+1} - \frac{i}{\hbar} M(t) \langle f_{2\uparrow}^v c_{\mathbf{k}1} \rangle_{+1} \\ &+ \frac{i}{\hbar} (\epsilon_{2\uparrow}^v - \epsilon_{2\uparrow}^c - \hbar\omega_{\mathbf{k}1} + 2\omega_L + i\gamma_{\text{PD}}\hbar) \langle p_{2\uparrow}^\dagger c_{\mathbf{k}1} \rangle_{+2} \end{aligned} \quad (\text{A.28})$$

$$\begin{aligned}
d_t \langle p_{\text{DEC}_{\mathbf{k}1}} \rangle &= -\frac{i}{\hbar} M(t) \langle p_{\text{II}c_{\mathbf{k}1}} \rangle_{+1} \\
&+ \frac{i}{\hbar} V \langle f_{1\downarrow}^v p_{2\uparrow} c_{\mathbf{k}1} \rangle - \frac{i}{\hbar} M_{2\uparrow}^{\mathbf{k}*} \langle p_{\text{II}} \rangle \\
&+ \frac{i}{\hbar} (\epsilon_{1\uparrow}^c + \epsilon_{1\downarrow}^c - \epsilon_{1\downarrow}^v - \epsilon_{2\uparrow}^v - \hbar\omega_{\mathbf{k}1} + i\gamma_{\text{PD}}\hbar) \langle p_{\text{DEC}_{\mathbf{k}1}} \rangle
\end{aligned} \tag{A.29}$$

$$\begin{aligned}
d_t \langle p_{\text{II}c_{\mathbf{k}1}} \rangle_{+1} &= -\frac{i}{\hbar} M(t) \langle p_{\text{DEC}_{\mathbf{k}1}} \rangle \\
&+ \frac{i}{\hbar} V (\langle f_{2\uparrow}^c f_{1\downarrow}^v c_{\mathbf{k}1} \rangle_{+1} - \langle f_{1\uparrow}^c f_{1\downarrow}^c c_{\mathbf{k}1} \rangle_{+1}) \\
&+ \frac{i}{\hbar} (\epsilon_{1\uparrow}^c + \epsilon_{1\downarrow}^c - \epsilon_{1\downarrow}^v - \epsilon_{2\uparrow}^c - \hbar\omega_{\mathbf{k}1} + \omega_L + i\gamma_{\text{PD}}\hbar) \langle p_{\text{II}c_{\mathbf{k}1}} \rangle_{+1}
\end{aligned} \tag{A.30}$$

$$\begin{aligned}
d_t \langle p_{\text{II}c_{\mathbf{k}1}}^\dagger \rangle_{+1} &= \frac{i}{\hbar} M(t) \langle p_{\text{DE}c_{\mathbf{k}1}}^\dagger \rangle_{+2} \\
&+ \frac{i}{\hbar} V (\langle f_{1\uparrow}^c f_{1\downarrow}^c c_{\mathbf{k}1} \rangle_{+1} - \langle f_{2\uparrow}^c f_{1\downarrow}^v c_{\mathbf{k}1} \rangle_{+1}) \\
&+ \frac{i}{\hbar} (\epsilon_{2\uparrow}^c + \epsilon_{1\downarrow}^v - \epsilon_{1\downarrow}^c - \epsilon_{1\uparrow}^c - \hbar\omega_{\mathbf{k}1} + \omega_L + i\gamma_{\text{PD}}\hbar) \langle p_{\text{II}c_{\mathbf{k}1}}^\dagger \rangle_{+1}
\end{aligned} \tag{A.31}$$

$$\begin{aligned}
d_t \langle f_{1\downarrow}^v p_{2\uparrow} c_{\mathbf{k}1} \rangle &= \frac{i}{\hbar} M(t) (\langle f_{2\uparrow}^v f_{1\downarrow}^v c_{\mathbf{k}1} \rangle_{+1} - \langle f_{2\uparrow}^c f_{1\downarrow}^v c_{\mathbf{k}1} \rangle_{+1}) \\
&+ \frac{i}{\hbar} V \langle p_{\text{DEC}_{\mathbf{k}1}} \rangle - \frac{i}{\hbar} M_{2\uparrow}^{\mathbf{k}*} \langle f_{2\uparrow}^c f_{1\downarrow}^v \rangle \\
&+ \frac{i}{\hbar} (\epsilon_{2\uparrow}^c - \epsilon_{2\uparrow}^v - \hbar\omega_{\mathbf{k}1} + i\gamma_{\text{PD}}\hbar) \langle f_{1\downarrow}^v p_{2\uparrow} c_{\mathbf{k}1} \rangle
\end{aligned} \tag{A.32}$$

$$\begin{aligned}
d_t \langle p_{\text{DE}c_{\mathbf{k}1}}^\dagger \rangle_{+2} &= \frac{i}{\hbar} M(t) \langle p_{\text{II}c_{\mathbf{k}1}}^\dagger \rangle_{+1} - \frac{i}{\hbar} V \langle f_{1\downarrow}^v p_{2\uparrow}^\dagger c_{\mathbf{k}1} \rangle_{+2} \\
&+ \frac{i}{\hbar} (\epsilon_{2\uparrow}^v + \epsilon_{1\downarrow}^v - \epsilon_{1\downarrow}^c - \epsilon_{1\uparrow}^c - \hbar\omega_{\mathbf{k}1} + 2\omega_L + i\gamma_{\text{PD}}\hbar) \langle p_{\text{DE}c_{\mathbf{k}1}}^\dagger \rangle_{+2}
\end{aligned} \tag{A.33}$$

$$\begin{aligned}
d_t \langle f_{2\uparrow}^c f_{1\downarrow}^v c_{\mathbf{k}1} \rangle_{+1} &= \frac{i}{\hbar} M(t) (\langle f_{1\downarrow}^v p_{2\uparrow}^\dagger c_{\mathbf{k}1} \rangle_{+2} - \langle f_{1\downarrow}^v p_{2\uparrow} c_{\mathbf{k}1} \rangle) \\
&+ \frac{i}{\hbar} V (\langle p_{\text{II}c_{\mathbf{k}1}} \rangle_{+1} - \langle p_{\text{II}c_{\mathbf{k}1}}^\dagger \rangle_{+1}) \\
&+ \frac{i}{\hbar} (-\hbar\omega_{\mathbf{k}1} + \omega_L) \langle f_{2\uparrow}^c f_{1\downarrow}^v c_{\mathbf{k}1} \rangle_{+1}
\end{aligned} \tag{A.34}$$

$$\begin{aligned}
d_t \langle f_{1\uparrow}^c f_{1\downarrow}^c c_{\mathbf{k}1} \rangle_{+1} &= +\frac{i}{\hbar} V (\langle p_{\text{II}c_{\mathbf{k}1}}^\dagger \rangle_{+1} - \langle p_{\text{II}c_{\mathbf{k}1}} \rangle_{+1}) \\
&+ \frac{i}{\hbar} (-\hbar\omega_{\mathbf{k}1} + \omega_L) \langle f_{1\uparrow}^c f_{1\downarrow}^c c_{\mathbf{k}1} \rangle_{+1}
\end{aligned} \tag{A.35}$$

$$\begin{aligned}
d_t \langle f_{2\uparrow}^v f_{1\downarrow}^v c_{\mathbf{k}1} \rangle_{+1} &= -\frac{i}{\hbar} M_{2\uparrow}^{\mathbf{k}*} \langle f_{1\downarrow}^v p_{2\uparrow}^\dagger \rangle_{+1} \\
&+ \frac{i}{\hbar} M(t) (\langle f_{1\downarrow}^v p_{2\uparrow} c_{\mathbf{k}1} \rangle - \langle f_{1\downarrow}^v p_{2\uparrow}^\dagger c_{\mathbf{k}1} \rangle_{+2}) \\
&+ \frac{i}{\hbar} (-\hbar\omega_{\mathbf{k}1} + \omega_L) \langle f_{2\uparrow}^v f_{1\downarrow}^v c_{\mathbf{k}1} \rangle_{+1}
\end{aligned} \tag{A.36}$$

$$\begin{aligned}
d_t \langle f_{1\downarrow}^v p_{2\uparrow}^\dagger c_{\mathbf{k}1} \rangle_{+2} &= -\frac{i}{\hbar} V \langle p_{\text{DE}c_{\mathbf{k}1}}^\dagger \rangle_{+2} \\
&+ \frac{i}{\hbar} M(t) (\langle f_{2\uparrow}^c f_{1\downarrow}^v c_{\mathbf{k}1} \rangle_{+1} - \langle f_{2\uparrow}^v f_{1\downarrow}^v c_{\mathbf{k}1} \rangle_{+1}) \\
&+ \frac{i}{\hbar} (\epsilon_{2\uparrow}^v - \epsilon_{2\uparrow}^c - \hbar\omega_{\mathbf{k}1} + 2\omega_L + i\gamma_{\text{PD}}\hbar) \langle f_{1\downarrow}^v p_{2\uparrow}^\dagger c_{\mathbf{k}1} \rangle_{+2}
\end{aligned} \tag{A.37}$$

* schulze@itp.tu-berlin.de

¹ W. Shockley and H. J. Queisser, J. Appl. Phys. **32**, 510 (1961).
² J. McClain and J. Schrier, J. Phys. Chem. C **114**, 14332 (2010).
³ T. Winzer, A. Knorr, and E. Malic, Nano Lett. **10**, 4839 (2010).
⁴ M. Califano, ACSNano **3**, 2706 (2009).
⁵ J. A. McGuire, M. Sykora, J. Joo, J. M. Pietryga, and V. I. Klimov, Nano Lett. **10**, 2049 (2010).
⁶ P. Tyagi and P. Kambhampati, J. Chem. Phys. **134**, 094706 (2011).
⁷ C. Delerue, G. Allan, J. J. H. Pijpers, and M. Bonn, Phys. Rev. B **81**, 125306 (2010).
⁸ A. Franceschetti, J. M. An, and A. Zunger, Nano Lett. **6**, 2191 (2006).
⁹ A. Shabaev, A. L. Efros, and A. J. Nozik, Nano Lett. **6**,

2856 (2006).
¹⁰ J.-W. Luo, A. Franceschetti, and A. Zunger, Nano Lett. **8**, 3174 (2008).
¹¹ G. Nair, S. M. Geyer, L.-Y. Chang, and M. G. Bawendi, Phys. Rev. B **78**, 125325 (2008).
¹² J. J. H. Pijpers, E. Hendry, M. T. W. Milder, R. Fanciulli, J. Savolainen, J. L. Herek, D. Vanmaekelbergh, S. Ruhman, D. Mocatta, D. Oron, et al., J. Phys. Chem. C **111**, 4146 (2007).
¹³ R. D. Schaller and V. I. Klimov, Phys. Rev. Lett. **92**, 186601 (2004).
¹⁴ W. M. Witzel, A. Shabaev, C. S. Hellberg, V. L. Jacobs, and A. L. Efros, Phys. Rev. Lett. **105**, 137401 (2010).
¹⁵ I. Kang and F. W. Wise, J. Opt. Soc. Am. B **14**, 1632 (1997).
¹⁶ F. Rossi and T. Kuhn, Rev. Mod. Phys. **74**, 895 (2002).
¹⁷ M.-R. Dachner, E. Malic, M. Richter, A. Carmele,

- J. Kabuss, A. Wilms, J.-E. Kim, G. Hartmann, J. Wolters, U. Bandelow, et al., *Phys. Status Solidi B* **247**, 809 (2010).
- ¹⁸ A. J. Nozik, M. C. Beard, J. M. Luther, M. Law, R. J. Ellingson, and J. C. Johnson, *Chem. Rev.* **110**, 6873 (2010).
- ¹⁹ J. Kabuss, S. Werner, A. Hoffmann, P. Hildebrandt, A. Knorr, and M. Richter, *Phys. Rev. B* **81**, 075314 (2010).
- ²⁰ J. J. H. Pijpers, E. Hendry, M. T. W. Milder, R. Fanciulli, J. Savolainen, J. L. Herek, D. Vanmaekelbergh, S. Ruhman, D. Mocatta, D. Oron, et al., *J. Phys. Chem. C* **112**, 4783 (2008).